PAPER • **OPEN ACCESS**

SARS-CoV-2 infection of 3D *in vitro* cardiac spheroids models the activation of antiviral, inflammatory, fibrotic, and contractile responses in a dose-dependent manner

To cite this article: Matt D Johansen *et al* 2026 *Biofabrication* **18** 015028

Biofabrication

OPEN ACCESS

RECEIVED
25 July 2024

REVISED
26 September 2025

ACCEPTED FOR PUBLICATION
1 December 2025

PUBLISHED
29 January 2026

PAPER

SARS-CoV-2 infection of 3D *in vitro* cardiac spheroids models the activation of antiviral, inflammatory, fibrotic, and contractile responses in a dose-dependent manner

Matt D Johansen[1,2,4,*], **Clara Liu Chung Ming**[1,3,4], **Philip M Hansbro**[1,2] **and Carmine Gentile**[1,3,*]

[1] University of Technology Sydney, Sydney, NSW, Australia
[2] Centenary Institute, Sydney, NSW, Australia
[3] Cardiovascular Regeneration Group, Heart Research Institute, Sydney, NSW, Australia
[4] Equally contributing first authors.
[*] Authors to whom any correspondence should be addressed.

E-mail: matt.johansen@uts.edu.au and carmine.gentile@uts.edu.au

Keywords: SARS-CoV-2, COVID-19, cardiac spheroids, myocardial damage, 3D *in vitro* modelling

Supplementary material for this article is available online

Abstract

The emergence of SARS-CoV-2 led to a global pandemic with severe respiratory symptoms and substantial extrapulmonary manifestations. Increasing evidence suggests significant cardiovascular complications associated with SARS-CoV-2 infection, which are critical factors in morbidity and mortality. In this study, we assessed the viral infectivity and viral niche of SARS-CoV-2 using our clinically-amenable *in vitro* cardiac spheroids (CSs), which have previously been demonstrated to be an optimal tool to recapitulate the complex cardiac pathophysiology. We examined the expression profiles of cardiovascular-related disease genes and pathways involved in inflammation, interferon responses, and antiviral defence following infection. Genes associated with apoptosis, chemotaxis, fibrosis, and contractile function exhibited substantial increases, implicating these pathways in the cardiac response to SARS-CoV-2. Furthermore, our 3D rendering analyses using confocal imaging revealed cell-specific effects mediated by the virus by colocalising SARS-CoV-2 nucleocapsid protein with each cell type, supporting the ability of CSs to facilitate viral replication and contributing to the observed phenotypes. Additionally, SARS-CoV-2 could only infect intact CSs, whereas it did not infect individual cell types cultured individually. The unique ability of CSs to model SARS-CoV-2 in the heart may potentially mirror the pathophysiological changes observed in COVID-19-induced cardiac complications. Altogether, our results suggest that CSs offer a valuable tool for dissecting direct host-viral interactions and advancing our understanding of SARS-CoV-2-related cardiac injury. Our findings underscore the utility of CSs in revealing the mechanisms of SARS-CoV-2-induced cardiac damage and provide a basis for further studies into the long-term cardiovascular consequences of SARS-CoV-2.

1. Introduction

The novel coronavirus, SARS-CoV-2, responsible for Coronavirus disease 2019 (COVID-19), first appeared in December 2019 and has since resulted in over >1 billion infections and >10 million deaths globally as of 2025. However, it is likely that this is much higher due to significantly reduced testing and reporting since the introduction of vaccination (Msemburi *et al* 2023). While pneumonia is the primary cause of hospitalisation due to SARS-CoV-2, other complications such as circulatory shock leading to organ dysfunction (8.7%), acute cardiac injury (7.2%), arrhythmias (16.7%), acute respiratory distress syndrome (ARDS, 19.6%), and acute kidney injury (3.6%) have been observed in COVID patients (Wang *et al* 2020). Acute cardiac injury is a prevalent and severe complication of severe SARS-CoV-2, increasing the likelihood of heart attacks and critical conditions among affected individuals,

such as acute myocarditis, acute coronary syndrome, arrhythmias and heart failure (Qiu *et al* 2023). Chen *et al* (2020) have shown a significant dysregulation of angiotensin-converting enzyme (ACE), which is a marker for heart failure diseases, in COVID-19 patients. Abnormal ACE signalling leads to the activation of inflammatory cascades and potentially leads to death in patients with diabetes and cardiovascular diseases (Maccio *et al* 2021). Importantly, even though vaccination against COVID-19 has significantly reduced the likelihood of clinical sequelae, cardiovascular disease, and all-cause mortality following SARS-CoV-2 infection, the long-term consequences following recovery from COVID-19 remain unknown (Lam *et al* 2024).

SARS-CoV-2 infection has been shown to trigger a strong immunological response, resulting in cytokine storm syndrome, which is characterised by the uncontrolled production of pro-inflammatory cytokines leading to ARDS and multiple organ failure (Li *et al* 2020, Lu *et al* 2024a). Plasma interleukin-6 (IL-6) has been associated with a significant reduction in CD4+ and CD8+ T cell populations, a high proportion of functionally exhausted T cells persisting after recovery from acute SARS-CoV-2 infection, increased hospitalisation rates, and higher all-cause mortality among COVID-19 patients (Lu *et al* 2022, Jamoussi *et al* 2023, Nikkhoo *et al* 2023). Furthermore, other studies have demonstrated that significant increases in IL-6 are linked to elevated blood pressure and a heightened risk of heart failure in SARS-CoV-2 patients. These factors have recently emerged as key predictors of cardiovascular complications in COVID-19 (Chen *et al* 2020, Nguyen *et al* 2022, Lu *et al* 2024b). However, it remains uncertain whether SARS-CoV-2 can directly infect the human heart and cause a productive infection, and which host-viral mechanisms influence cardiac function. Despite recent advancements in bioengineered heart tissue models, *in vitro* human cell-based viral models are still lacking in fully recapitulating the complex microenvironment required for successful infection. As such, we assessed the viral infectivity and niche of SARS-CoV-2 using our clinically amenable *in vitro* cardiac spheroids (CSs). CSs have been shown to better mimic the molecular, cellular, and extracellular features of the human heart microenvironment that recapitulate the complex cardiac pathophysiology typical of ischemia-reperfusion injury, doxorubicin-induced cardiotoxicity, and post-partum cardiovascular health (Polonchuk *et al* 2017, Sharma *et al* 2022b, Chung Ming *et al* 2024). CSs are generated by co-culturing the primary cell types found in the human heart—cardiomyocytes, endothelial cells, and fibroblasts—in ratios that closely mimic their natural proportions. These CSs have demonstrated remarkable regenerative potential when transplanted into an *in vivo* mouse model of myocardial infarction (Roche *et al* 2023) and have been used as a drug screening model, demonstrating the cardioprotective effect of acetylcholine-loaded nanoparticles against doxorubicin-induced cardiotoxicity in CSs (Liu Chung Ming *et al* 2025), establishing them as a robust and representative model of the human heart.

Therefore, we hypothesised that CSs could be used to study the host-viral mechanisms of SARS-CoV-2 in the heart, facilitating the identification of early cardiovascular changes at the cellular and molecular level during infection and post-infection. In this study, we evaluated the impact of SARS-CoV-2 infection over 7 d on the viral niche, cardiovascular disease markers, and expression of key pro-inflammatory cytokines.

2. Methods

2.1. Cell culture and CS formation

CSs and cells were prepared according to our previously published protocols (Sharma *et al* 2022a). Briefly, human coronary artery endothelial cells (HCAECs) were cultured in MesoEndo Media (Sigma-Aldrich, Missouri, USA) and human cardiac fibroblasts (HCFs) were cultured in Cardiac Fibroblast Growth Media (Sigma-Aldrich, Missouri, USA) both supplemented with 1% penicillin/streptomycin (Thermo Fisher Scientific, Massachusetts, USA) and 1% L-glutamine (Thermo Fisher Scientific, Massachusetts, USA). Media was changed every 2 d and cells were cultured until 80%–90% confluency before being passaged using Trypsin-EDTA 25% (Sigma-Aldrich, Missouri, USA). A cryovial of iCell® Cardiomyocytes (iCells) (5×10^6 cells; Cellular Dynamics, Wisconsin, USA) was thawed and transferred to a fibronectin (Sigma-Aldrich, Missouri, USA)-precoated T-75 tissue flask and incubated overnight with iCell Plating Media at 37 °C and 5% CO_2, following the manufacturer's guidelines. After 20 h, media was replaced with iCell Maintenance Media and after 72 h, iCells were detached with TryplE (Thermo Fisher Scientific, Massachusetts, USA) for CSs formation, while other HCAECs, HCFs and iCells were individually plated in a 24-well plate in monolayer cultures (100, 000 cells per well).

Prior to CS formation, agarose powder (Sigma-Aldrich, Missouri, USA) and 3D micromoulds (Sigma-Aldrich, Missouri, USA) were sterilised under UV for 30 min. Agarose powder (0.2%) was reconstituted in phosphate buffered saline (PBS) solution and heated for 60 s to allow proper dissolution of the powder. The solution was pipetted into 3D micromoulds to form moulds, and after a few seconds, the solidified moulds were submerged in culture media and incubated at 37 °C and 5% CO_2, following the manufacturer's guidelines.

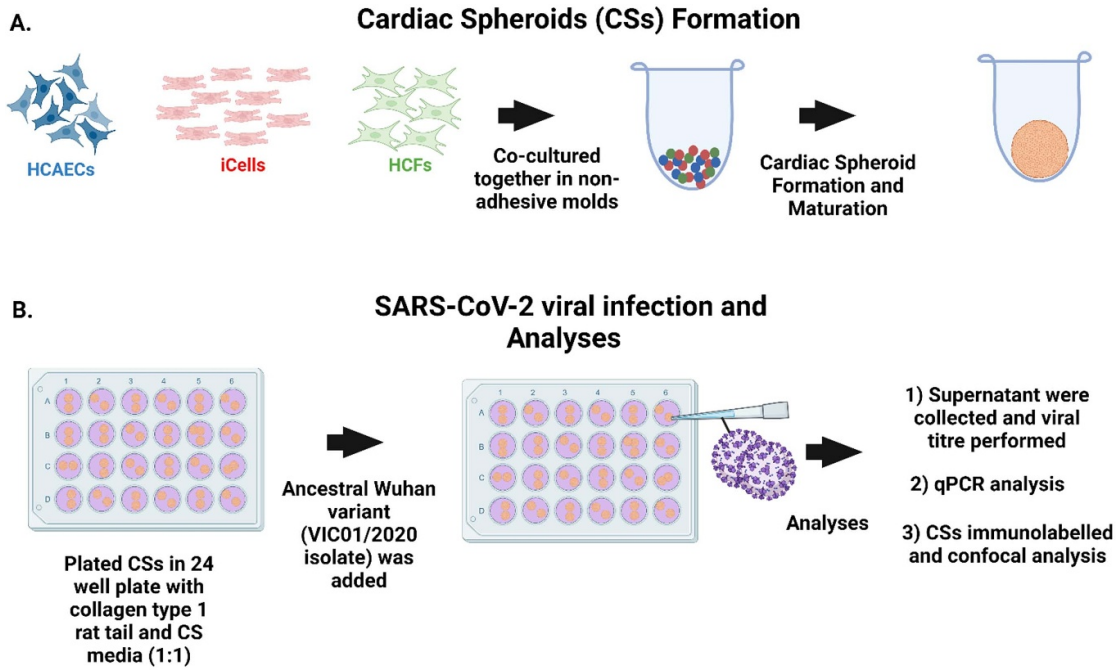

Figure 1. Schematic illustration of CS formation and analyses of SARS-CoV-2 post-viral infection. (A) HCAECs, iCells, and HCFs were co-cultured in 3D Petri dish moulds till fully formed CSs were observed. (B) After their formation, CSs were plated in a 24-well plate with collagen type 1 rat tail and CS media at a ratio of 1:1. Ancestral Wuhan variant VIC01/2020 isolate was then added. The analyses of post-viral infections were: 1) viral titre; 2) qPCR analyses; and 3) CS immunolabelling and confocal analyses.

After the three cell types were detached from their respective flasks, they were counted and mixed in a ratio of 2:1:1 (iCells: HCAECs: HCFs). As illustrated in figure 1(A), cell pellets were resuspended in CS culture media (iCell: HCAEC: HCF Media at a ratio of 2:1:1, respectively). A cell suspension (190 μl) was added to the inner cavity of each agarose mould and incubated at 37 °C and 5% CO_2 with daily media changes. Following 48 h, CS were collected and carefully transferred to a 24-well plate (a minimum of five CSs per well) as shown in figure 1(B). Collagen 1 rat tail (Merck, Massachusetts, USA) hydrogels were added on top of either CSs or individually plated cells before infection with SARS-CoV-2 virus.

2.2. SARS-CoV-2 viral infection

CSs were transported from UTS to the Centenary Institute for SARS-CoV-2 infection in a physical containment level 3 (PC3) facility. SARS-CoV-2 infection was performed using the ancestral Wuhan variant (VIC01/2020 isolate) (figure 1(B)). First, the culture medium was removed from each well and replaced with MEM media containing SARS-CoV-2 at a multiplicity of infection (MOI) of 0.1 or 1 (virus: cell), depending on the experiment performed. Unless otherwise specified, CS infection experiments used MOI 1 for all infections. Following 2 h of infection with gentle tilting of the plate every 15 min, the supernatant was discarded, and the CSs were gently washed with PBS twice to remove any extracellular virus floating in the media. Then, CS media without any virus was added back to each well and placed back in the incubator. Each day, the supernatant was collected and stored at −80 °C for downstream viral titre analyses, and the media was replaced in each well. At the end of the experiment, CSs were collected and resuspended in either 1 ml of neutral-buffered formalin (Sigma-Aldrich, Missouri, USA) or 1 ml of TRIZOL (Sigma-Aldrich, Missouri, USA) and stored either at room temperature or at −80 °C, respectively, for further processing.

2.3. Immunolabelling and confocal imaging

Post-fixation, CSs were washed three times with PBS containing 1% sodium azide (PBSA) and permeabilised with 0.2% Triton X-100 for 30 min. Then 3% bovine serum albumin (BSA)/PBSA was added overnight at 4 °C. CS were then probed with CD31 (1:10, BD Biosciences, Franklin Lakes, USA) and anti-SARS-CoV-2 Nucleocapsid (1:10, Sigma-Aldrich, Missouri, USA) primary antibodies and incubated at 4 °C overnight. Following washing, goat anti-rabbit IgG H&L (Alexa Fluor® 647, Jackson ImmunoResearch, Pennsylvania, USA) and Goat Anti-Mouse IgG (H + L) (Alexa fluor® 790, Jackson ImmunoResearch, Pennsylvania, USA) secondary antibodies were added and incubated at 4 °C overnight. CSs were then incubated with vimentin (1:250, Abcam, Cambridge, UK) and Troponin C (1:10, Santa Cruz, California, USA)

primary-conjugated antibodies and Hoechst stain (10 μg ml^{-1}, Invitrogen, Massachusetts, USA) at 4 °C overnight. Finally, CS were washed three times with PBSA and stored at 4 °C before imaging.

Laser scanning confocal microscopy images were acquired using a Leica Stellaris 8 confocal with a 20X objective with a numerical aperture of 1.45 and Nyquist sampling. *Z* stacks were obtained with 0.9 μm optical slices, utilising a 1 AU pinhole. *Z* stacks were processed for 3D rendering visualisation using IMARIS software (Oxford Instruments plc, RRID:SCR_007370), and the three cell types were colocalised against Anti-SARS-CoV-2 Nucleocapsid.

2.4. RNA extraction and qPCR for human cardiovascular disease markers and targeted inflammation and interferon-related gene expression

RNA was isolated using the guanidine-isothiocyanate lysis technique, employing the RNeasy Mini Kit (Qiagen, Hilden, Germany). The process involved lysing and homogenising the samples in absolute ethanol (100% v/v) to create optimal conditions for binding, followed by loading onto the RNeasy silica membrane. The total RNA quantity was determined by measuring the A260/280 ratios in 10 mM Tris·Cl, pH 7.5. For each sample, 20 ng of RNA was reverse-transcribed into cDNA using the RT^2 First Strand Kit (Qiagen, Hilden, Germany), then diluted for the RT^2 SYBR Green qPCR Master Mix (Qiagen, Hilden, Germany).

The RT^2 Profiler PCR Arrays (Qiagen, Hilden, Germany), designed specifically for human cardiovascular disease markers such as angiogenesis, fibrosis, inflammation, cytoskeletal proteins, cell cycle-related proteins, and apoptosis, were used for qPCR, utilising the Quantstudio 12K Flex Real-Time PCR System (Thermo Fisher Scientific, Massachusetts, USA). Data analysis was performed with Qiagen's web-based software, applying the fold-change ($\Delta\Delta Ct$) method.

For targeted inflammation and interferon-related gene expression analyses, qRT-PCR was performed using iTaqTM Universal SYBR® Green Supermix (Bio-Rad) and a CFX384 Touch Real-Time PCR Detection System (Bio-Rad) and analysed with CFX Maestro Software V2.1 (Bio-Rad). Primer sequences used in this study were designed and purchased from Sigma-Aldrich from their KiCqStart™ readymade primer pairs.

2.5. Statistical analysis

Data were analysed using Graphpad Prism software to calculate mean ± SEM and one-way ANOVA test (Turkey multiple comparison) to compare every sample. Significance was set to $p < 0.05$. For gene expression qPCR analyses, fold changes were calculated as 2 ($-\Delta\Delta Ct$) method (Livak and Schmittgen 2001).

3. Results

3.1. SARS-CoV-2 viral replication is dose-dependent with peak titres at 3 d post-infection

To assess the suitability of CSs as a 3D *in vitro* human cardiac model for SARS-CoV-2 infection, we examined different MOI at 0.1 and 1 (viral PFU:cell). Following SARS-CoV-2 infection, the viral inoculum was removed, and media were replaced daily for profiling viral titres across time. As shown in figure 1, MOI 0.1 showed highly variable viral replication throughout the infection period, with several samples falling below the limit of detection (LOD). Comparatively, MOI 1 had more consistent viral replication and showed a peak at day 3 post-infection, with a significant difference at 3 d post-infection as compared to MOI 0.1 (figure 2).

LOD represents control compared with MOI 0.1 and MOI 1. Data are presented as individual points and mean ± SEM. LOD represents LOD for viral titres is set to 40 PFU/ml. Statistical significance is denoted as $P > 0.05$ = ns and $P < 0.05$ = *, analysed using a one-way ANOVA with a Tukey's multiple comparisons test ($N > 2$).

3.2. SARS-CoV-2 viral infectivity is significant in CSs at day 3

Building on our earlier findings that CSs are a viable *in vitro* platform for SARS-CoV-2 infection, we next wanted to determine which of the individual cardiac cell populations can act as a viral niche that promotes SARS-CoV-2 replication. To do this, we examined all three cell types individually in a monolayer culture suspended in collagen hydrogels (HCF, HCAEC, and iCells) and compared these results to CSs. Our findings revealed no detectable viral infectivity in individually cultured HCFs in monolayers, with virus only detectable at day 1 post-infection, which likely represents residual virus present in the media from the infection (figure 3(A)). Further, HCAECs and iCells revealed a significant reduction in SARS-CoV-2 at 2 d post-infection, with no detectable virus present from day 3 post-infection (figures 3(B) and (C)). Conversely, when these three cell types were combined in CSs, there was notable SARS-CoV-2 replication, with a peak of viral replication present at day 3 post-infection, which significantly increased between day 1 and day 3 post-infection, suggestive of a productive and robust infection (figure 3(D)). A comparative analysis of all samples demonstrated that SARS-CoV-2 was significantly higher in CSs at day 2 post-infection as compared to both HCAEC and iCells and

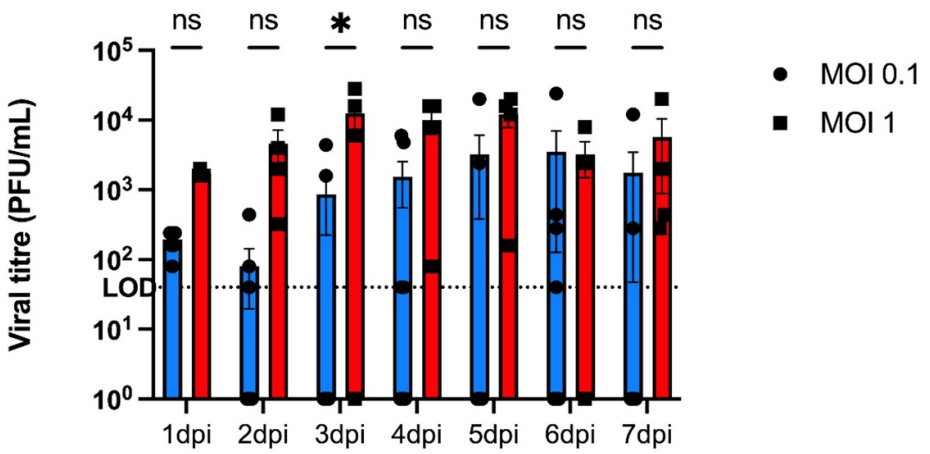

Figure 2. Viral titre of CS exposed to different MOI of SARS-CoV-2 across a seven-day infection.

was not detectable in HCFs at day 2 post-infection (figure 3(E)). Taken together, our findings demonstrate that SARS-CoV-2 does not infect the individual cell types that comprise CSs. Nevertheless, the complex microenvironment and crosstalk of these three cell types in CSs results in notable viral replication at day 3 post-infection.

3.3. SARS-CoV-2 nucleocapsid infects HCFs and iCells in CSs through 3D rendering analysis

Having identified that SARS-CoV-2 can replicate in CSs, while individual cell types do not allow support viral replication, we next wanted to evaluate which cells were infected in CSs using 3D rendering analyses of CSs stained with antibodies against each cell type, as well as the SARS-CoV-2 nucleocapsid (N) protein (figures 4 and 5 and supplementary figure S1). Figure 4 depicts our observations for both day 3 and day 7 following SARS-CoV-2 infection. Our findings reveal a notable presence of the SARS-CoV-2 N protein within vimentin-positive HCFs (green) and cardiac Troponin T-positive iCells (red) at both examined timepoints. Additionally, the presence of the SARS-CoV-2 N protein was detected in CD31-positive HCAECs (blue) at day 7 (supplementary videos S1-4).

3.4. SARS-CoV-2 impairs cardiovascular disease-related gene expression in CSs

Given our earlier findings that SARS-CoV-2 can cause a productive infection in CSs, we next investigated the impact of SARS-CoV-2 infection on the relative expression of genes relevant to cardiovascular health. These include genes regulating apoptosis, ACE, fibrosis, and contractility at day 7 post-infection (figure 6). We measured a significant increase in the expression of Annexin A4 (ANXA4), an apoptosis-related gene, at MOI 1, while its expression was decreased at MOI 0.1 (figure 6(A)). This could indicate that SARS-CoV-2 at different concentrations differentially regulates apoptotic-related dysfunction in CSs. Expression of the chemokine (C–C motif) ligand (CCL2s), which is responsible for monocyte recruitment, was significantly increased at MOI 1, while it did not significantly change at MOI 0.1 (figure 6(B)). Furthermore, a decrease in ACE gene expression, responsible for normal cardiac function and regulation of blood pressure, was identified across all SARS-CoV-2 infected groups (MOI 0.1 and 1) when compared to the control, which is media only (figure 6(C)). Moreover, the expression of collagen type I alpha 1 chain (COL1A1), a key cardiac fibrosis-related gene, was significantly reduced in all SARS-CoV-2 infected groups (MOI 0.1 and 1) (figure 6(d)). Finally, we measured a significant decrease in troponin T2 (TNNT2) and myosin heavy chain 6 (MYH6) gene expression, both responsible for cardiac muscle contraction, in all infected groups (figure 6(E)and (F). These findings demonstrate that SARS-CoV-2 infection modulates the expression of key cardiovascular genes involved in apoptosis, inflammation, fibrosis, and contractility within CSs, and closely mimics clinically relevant disease features observed in COVID-19 patients.

3.5. Effect of SARS-CoV-2 on relative expression of cytokines in the CS model

Finally, we evaluated the impact of SARS-CoV-2 on pro-inflammatory cytokines, interferons, and antiviral gene expression within CSs at days 3 and 7 following SARS-CoV-2 infection at MOI 1. Cytokines are essential for initiating immune responses, which contribute to both the protection of the host from viral infection as well as detrimental outcomes following infection, including tissue damage and mortality. We measured no significant changes in *IL1B* levels at

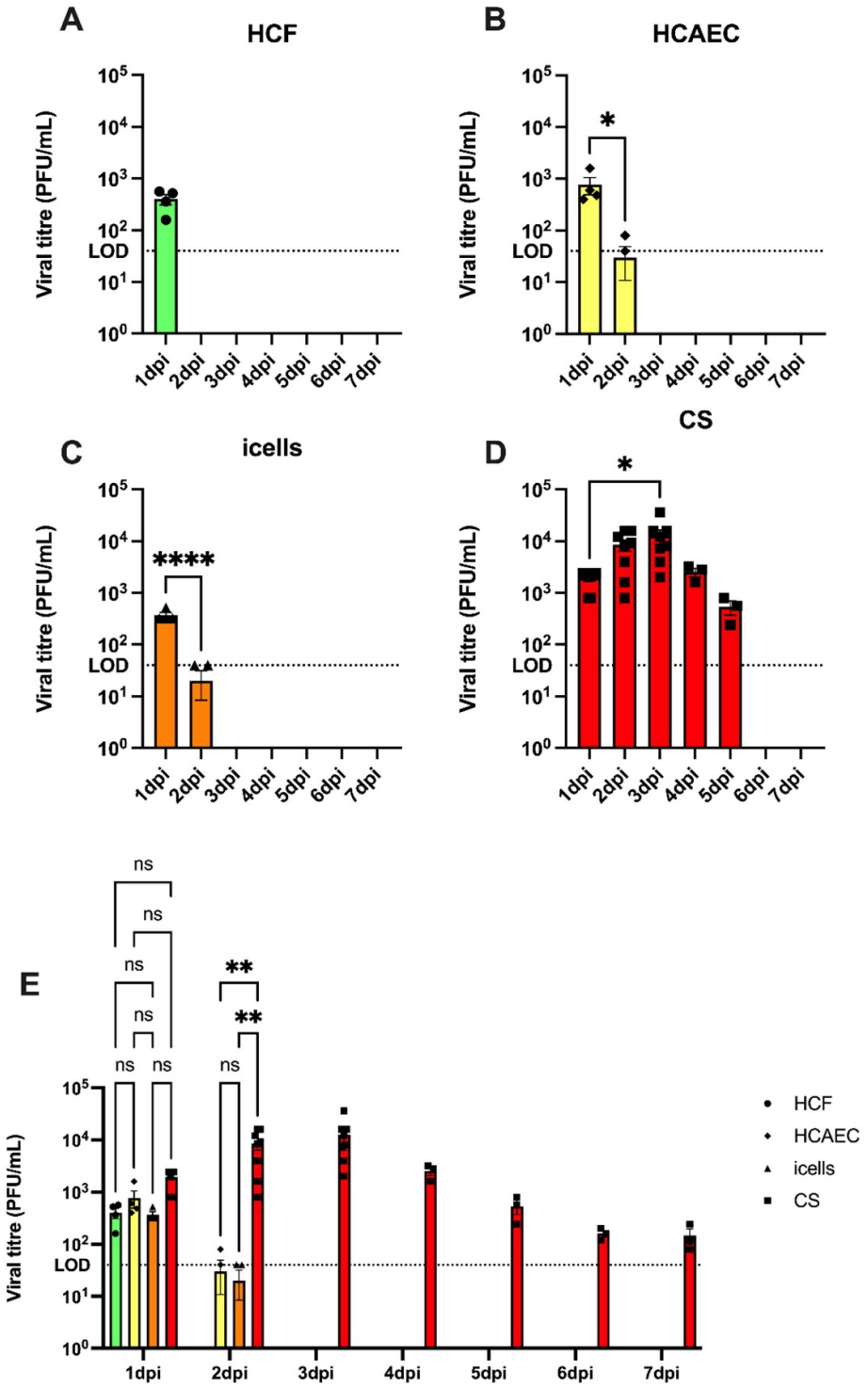

Figure 3. SARS-CoV-2 infectivity of individual cell types in monolayer cultures and CSs over a 7 d infection following infection with MOI 1. (A) HCFs, (B) HCAECs, (C) iCells, (D) CSs, and (E) comparative analysis of (A)–(D). Data is presented as individual points and mean ± SEM. LOD represents limit of detection for viral titres represents 40 PFU/ml^{-1}. Statistical significance is denoted as $P < 0.05 = *$, $p < 0.01 = **$, and $p < 0.0001 = ****$. Panels A–D were analysed using a one-way ANOVA followed by Tukey's multiple comparisons test ($N > 3$), while panel (E) was analysed using a two-way ANOVA followed by a Tukey's multiple comparison test ($N > 3$).

both day 3 and day 7 post-infection (figure 7(A)), in comparison to control CSs. On day 3 and day 7 post-infection, *IL6* levels remained unchanged in infected CS (figure 7(B)). Comparatively, examination of interleukin 1 receptor type 1 (*IL1R1*) showed a significant increase in infected CSs by day 7 post-infection (figure 7(C)). We also observed non-significant increases in Chemokine (C–X–C motif) ligand 1 (*CXCL1*) expression at day 3 post-infection, and a reduction back to baseline expression by day 7 post-infection as compared to uninfected CSs (figure 7(D)).

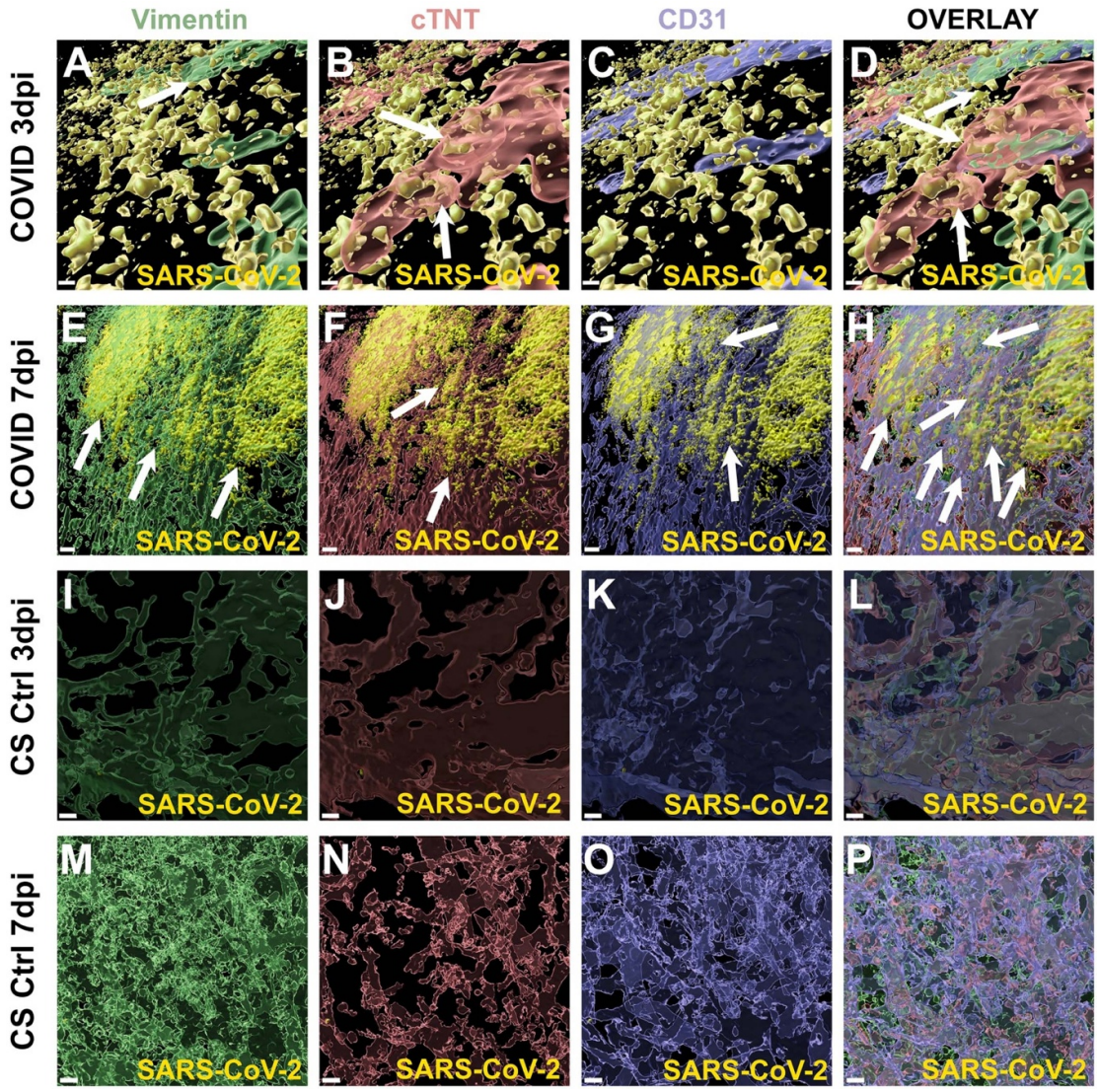

Figure 4. Colocalisation of SARS-CoV-2 N and cardiac cell markers in CSs using IMARIS software following SARS-CoV-2 infection with MOI 1. (A)–(P) All CSs were immunolabelled with CD31 (blue) to stain HCAEC, vimentin (green) to stain HCF, cTNT (red) to stain iCells and SARS-CoV-2 N (yellow) ($N > 3$). Red arrows depict the colocalisation between SARS-CoV-2 and the cardiac cells. (A)–(H) SARS-CoV-2 nucleocapsid (N) was present in HCFs and iCells at day 3 post-infection (A)–(D), and in HCAECs as well at day 7 post-infection (E)–(H). Scale bars equal 10 μm for COVID 3dpi (A)–(D), 30 μm for COVID 7dpi (E)–(H), 8 μm for ctrl 3dpi (I)–(L), and 15 μm for ctrl 7dpi (M)–(P), respectively.

We measured a significant increase in the expression of both interferon-beta (*IFNB1*) at day 3 and no significant changes in interferon gamma (*IFNG*) at both day 3 and day 7 post-infection compared to uninfected CSs (figures 7(E) and (F)). Further, there were no differences in the expression of Interferon Regulatory Factor 7 (*IRF7*) at both day 3 and day 7 post-infection (figure 7(G)). Interestingly, we measured significant increases in the expression of antiviral genes 2′-5′-oligoadenylate synthetases (OAS) in infected CSs, with significant increases in both *OAS2* and *OAS3* expression levels at day 7 post-infection (figures 7(H) and (I)). However, the antiviral gene MX Dynamin Like GTPase 2 (*MX2*) did not significantly change in expression levels at both day 3 and 7 post-infection (figure 7(J)).

4. Discussion

In this study, we explored the impact of SARS-CoV-2 infection on the heart tissue utilising our 3D *in vitro* CS model, which recapitulates important cardiovascular disease phenotypes that are directly translatable to human patients (Figtree *et al* 2017, Polonchuk *et al* 2017, Sharma *et al* 2022b). Firstly, we identified for the first time that CSs are suitable *in vitro* models that support SARS-CoV-2 replication in a dose-dependent manner. Furthermore, we showed that CSs are essential to support SARS-CoV-2 infectivity, with the individual cell types each demonstrating high-level resistance to infection despite the high viral infection dose used. Finally, we examined cardiovascular-related disease genes

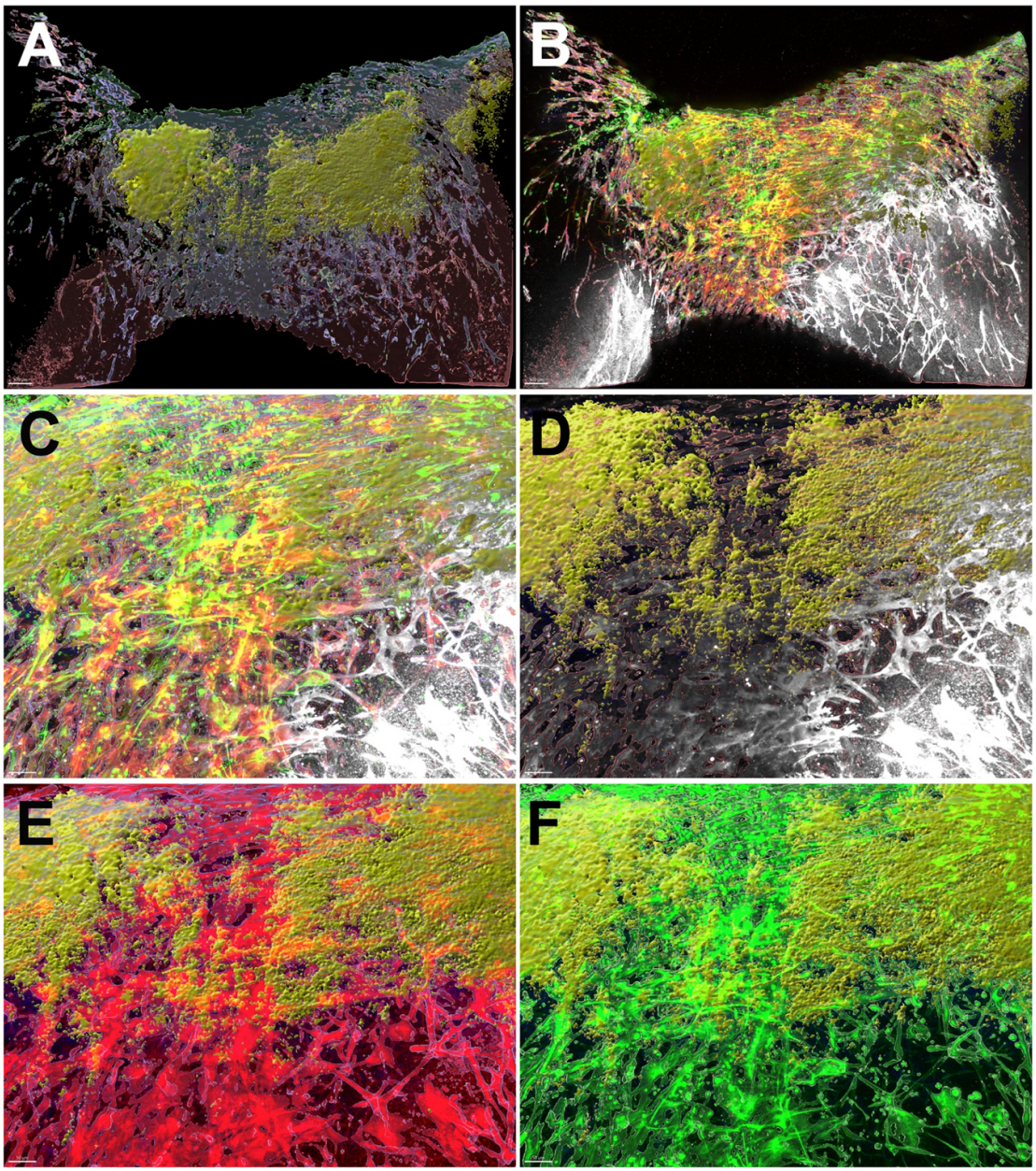

Figure 5. 3D rendered surfaces and confocal images of a cardiac spheroid infected with MOI 1 SARS-CoV-2 virus 7 d post infection. Overall (A) and (B) and side close-up (C)–(F) views of a cardiac spheroid infected with SARS-CoV-2, stained with antibodies against SARS-CoV-2 N protein (yellow). To verify the validity of the 3D rendered surfaces, we show the 3D rendered images of the cardiac spheroid stained with antibodies against cTNT (red), vimentin (green) and CD31 (blue) in each panel. We also show the confocal raw data (B)–(F) used for the generation of the 3D rendered surfaces, which are stained in white for CD31 (B)–(D), red for cTNT (B), (C) and (E), and green for vimentin (B), (C) and (F). These images are taken from supplementary video 4.

as well as inflammatory, interferon, and antiviral gene expression profiles in CS following SARS-CoV-2 infection and showed that there are significant changes to gene expression profiles, demonstrating that CSs are responsive to SARS-CoV-2 infection with a direct impact on antiviral, inflammatory, fibrotic, and contractility responses. Collectively, our findings show for the first time that CSs are a reliable and suitable model to examine the impact of SARS-CoV-2 infection in the heart, with the potential to pave the way to improve our understanding of the role of SARS-CoV-2 infection on the cardiovascular system, as well as to prevent its cardiovascular effects in patients. Future studies might focus on the evaluation of cardioprotective therapies against SARS-CoV-2 infection, as well as on a variety of additional viral-induced cardiac damage.

SARS-CoV-2 typically infects via the respiratory system, binding to epithelial cells in the nasal passages, as well as the upper and lower airways (Johansen *et al* 2020, Mulay *et al* 2021). In this study, we have shown that SARS-CoV-2 is able to directly infect cardiac cells in CSs and cause a productive and reproducible infection, with peak viral

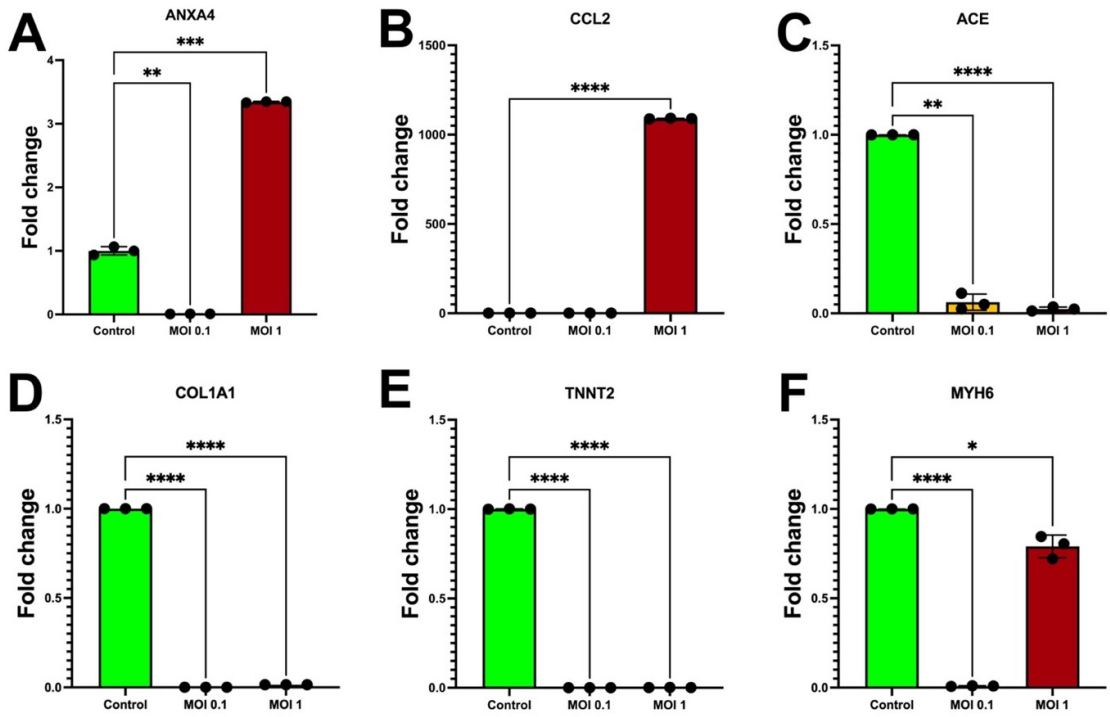

Figure 6. MOI 0.1 and MOI 1 SARS-CoV-2 infection regulates the expression of genes regulating apoptosis, inflammation, ACE signalling, and fibrosis in CS. Data shown as the fold change (3 replicates per sample) of infected CSs relative to control CSs and normalised to the expression of four housekeeping genes (Qiagen's web-based software). Statistical significance is denoted as $p < 0.05 = *$, $p < 0.01 = **$, and $p < 0.001 = ***$, analysed using paired one-way ANOVA followed by Tukey's multiple comparisons test.

titres at 3 d post-infection and low viral replication and/or clearance from day 5 post-infection onwards. These findings are consistent with others in primary bronchoepithelial cells from human patients, which show that viral replication and inflammatory responses peak from day 3 post-infection onwards and are often much higher in patients with co-morbidities such as those with chronic obstructive pulmonary disease (Johansen *et al* 2022). As such, it is plausible that CSs generated from patient-derived cells with cardiovascular disease may also recapitulate higher viral titres and greater inflammatory responses, as has been seen for other disease states in the lung. Nevertheless, this requires further investigation and was beyond the scope of this study.

To delineate the viral niche of SARS-CoV-2 infection in our CSs, we attempted to infect the individual cell types (HCFs, HCAECs, iCells) with SARS-CoV-2. Surprisingly, each of these individual cell types were not permissive to SARS-CoV-2 infection, with daily decreasing titres and complete viral clearance by day 2 post-infection. Interestingly, when we further explored host-viral interactions using 3D rendering analyses of colocalised cell markers and SARS-CoV-2 N protein in CSs, we identified that HCFs and iCells presented bound SARS-CoV-2 N protein at days 3 and 7 post-infection, while HCAECs only presented N protein from day 7 post-infection. Previous studies have shown that N protein accumulates around endoplasmic reticulum membranes that contain viral RNA replication sites (Scherer *et al* 2022), suggesting that SARS-CoV-2 may indeed be able to replicate in these individual cell types, and that the interaction of each of these cells typical of the complex microenvironment in CSs is required to support SARS-CoV-2 replication (Cawood *et al* 2007, Gao *et al* 2021). The differential temporal dynamics of N protein presence among the different cell types could reflect varying susceptibilities and responses to SARS-CoV-2 infection, emphasising the complexity of host-viral interactions with cardiac cell populations. To identify the mechanisms responsible for these phenomena requires further investigation. It has been increasingly recognised that cardiac-associated injuries are prevalent in patients recovering from acute SARS-CoV-2 infection and in those who develop long COVID-19 (Crespo-Barrios, Hanson *et al* 2022). Using our CS model, we identified significant upregulation of cardiac injury-associated genes. Apoptosis-related gene *ANXA4* was significantly increased, indicating that SARS-CoV-2 infection led to cell death in CSs. This is similar to what was previously reported, that SARS-CoV-2 proteins interact with ANXA4, ANXA1, ANXA5, with an effect on cell metabolism (Li *et al* 2023). Moreover, our results showed a significant overexpression of chemoattractant cytokine *CCL2*, suggestive of increased monocyte recruitment, which

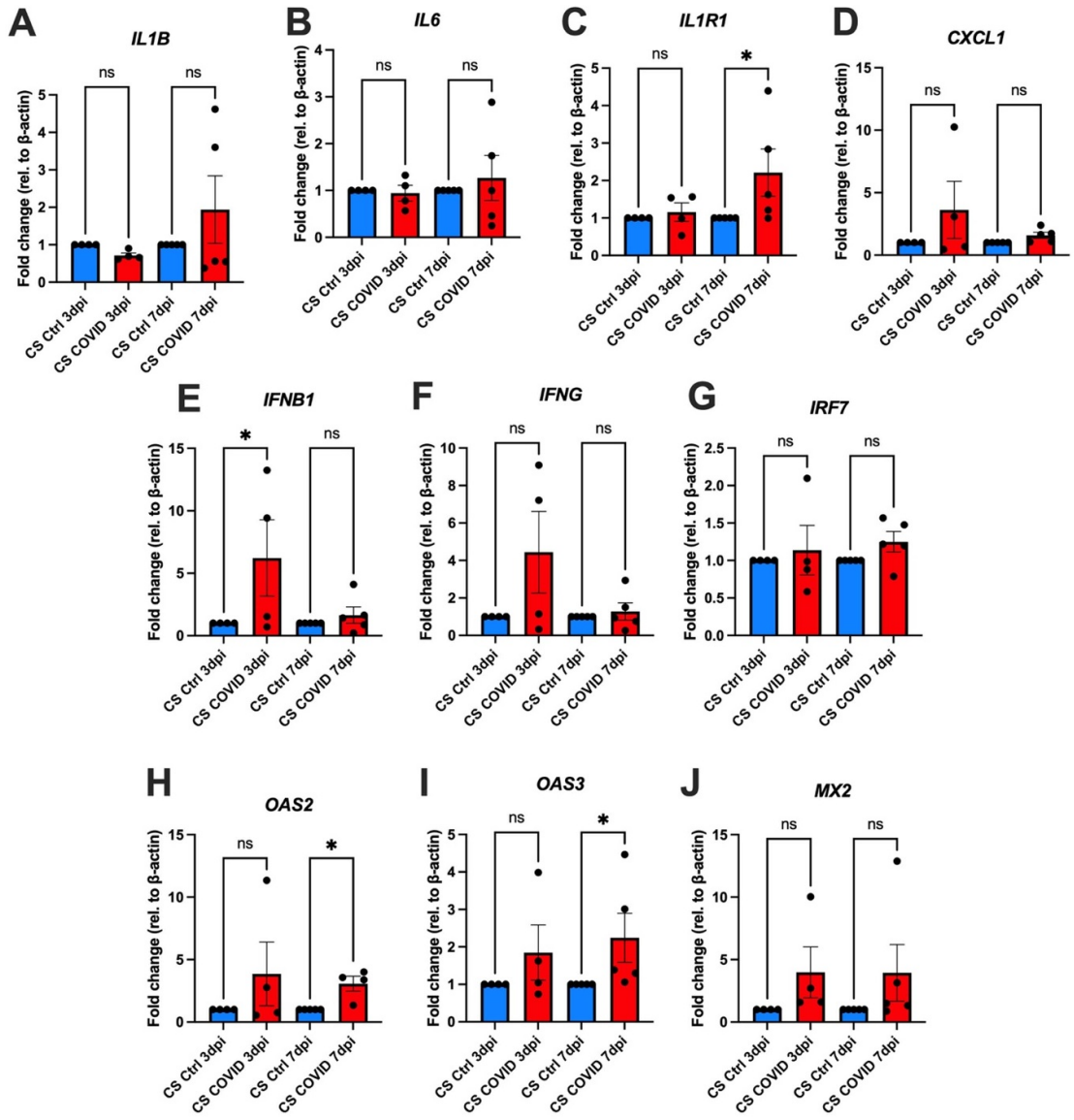

Figure 7. Pro-inflammatory, interferon, and antiviral gene expression of MOI 1 SARS-CoV-2 infected CSs at day 3 and day 7 post-infection compared to control CSs (media only condition). Data shown as the fold change of infected CSs relative to control CSs and normalised to the expression of housekeeping gene Beta-actin (β-actin). Data are presented as individual points and mean $\pm$ SEM. Statistical significance is denoted as $p > 0.05 =$ ns, $p < 0.05 = *$, $p < 0.01 = **$, and $p < 0.001 = ***$, analysed using paired one-way ANOVA followed by Tukey's multiple comparisons test ($N > 3$).

is important for host control of SARS-CoV-2 infection (Yang *et al* 2021b). Additionally, *ACE* expression is significantly downregulated following SARS-CoV-2 infection, which suggests that altered blood pressure and increased prevalence of cardiovascular disease may arise from acute SARS-CoV-2 infection. Numerous studies have found a significant dysregulation of ACE signalling post SARS-CoV-2 infection, which could thereby cause or aggravate cardiac damage. This could be due to weakened vasodilation, blood pressure reduction, and enhanced oxidative stress, which would lead to heart failure (Chen *et al* 2020, Verdecchia *et al* 2020, Li *et al* 2021, Sato *et al* 2021). We also found a significant downregulation of *COL1A1* similar to what was reported in previous studies (Mills *et al* 2021, Shao *et al* 2022). COL1A1 is a common marker for fibroblasts and has a crucial role in regulating collagen production and extracellular matrix proteins, leading to cardiac remodelling. Increased *COL1A1* expression is used as a biomarker for cardiac fibrosis following established heart failure. Nevertheless, we found that *COL1A1* was downregulated following SARS-CoV-2 infection, suggesting modulation of uncharacterised post-viral recovery pathways that may contribute to long-term cardiovascular sequelae in COVID-19 patients (Hua *et al* 2020). Furthermore, post-SARS-CoV-2 infection inhibited TNNT2 and MYH6 contractile gene expressions, leading to cardiomyocyte cell death, essential for the physiological contractile function

of the heart to pump blood throughout the body (Shen *et al* 2023).

Recent studies have shown that inflammation-induced cardiac dysfunction is driven by immune-cardiac cell interactions following SARS-CoV-2 infection in a human cardiac tissue model (Lu *et al* 2024a). Using our 3D *in vitro* CS model, we demonstrated no significant changes in *IL1B* and *IL6* expression at days 3 and 7 post-infection, suggesting that co-culture with immune cells such as macrophages may be required for robust pro-inflammatory gene expression, which is supported by previous studies (Yang *et al* 2021a). Interestingly, we observed a significant increase in *IL1R1* expression at day 7 post-infection, with previous studies demonstrating that increased *IL1R1* mediates acute inflammatory pathology while increasing survival from viral infection (Schmitz *et al* 2005). In this study, we did not see a significant increase in interferon-associated genes (*IFNG*, *IRF7*) but saw a significant abundance of *IFNB1* expression at day 3 post-infection. Moreover, we measured elevated *OAS2* and *OAS3* antiviral gene expression at day 7 post-infection. These findings agree with earlier studies, which have shown that OAS family genes are significantly elevated in SARS-CoV-2-infected cardiomyocytes and COVID-19 heart failure (Gao *et al*, 2023). Interestingly, these findings show that CSs can directly activate an antiviral state in response to SARS-CoV-2 infection, independent of neighbouring immune cell populations.

However, there were limitations to the current study. Firstly, infectivity of the CSs was largely viral dose-dependent, which has important implications for the applicability of our finding that CSs can support SARS-CoV-2 viral replication. Further, a major limitation was the inability to assess the contractile activity of CSs to demonstrate functional decreases in cardiac contractility associated with SARS-CoV-2 infection. This was due to physical limitations associated with the transfer of samples out of the physical containment level 3 (PC3/BSL3) facility, where the infection experiments were conducted, to our laboratories to perform functional analyses. As the CSs could only leave the PC3 facility if they were formalin-fixed or after mRNA extraction, this ultimately prevented direct evaluation of their contractile activity. While such inferences can be ascertained based on our gene expression profiling and 3D rendering, future studies should investigate the functional shifts in contractility in CSs associated with acute SARS-CoV-2 infection and following viral clearance. Finally, future studies may use either *ex vivo* human heart biopsies or plasma isolated from blood from SARS-CoV-2 infected patients to compare the expression levels of genes critical in cardiac injury following infection *in vitro* and *in vivo*, as well as to potentially explore any paracrine effects on the cardiac tissue, respectively. This would enhance the validation of the model, as well as it will provide a new tool to study short- and long-term effects of SARS-CoV-2 virus on the cardiac tissue.

5. Conclusion

In summary, our findings show for the first time that our 3D *in vitro* CS model is a suitable model for SARS-CoV-2 infection and for examining direct host-viral interactions, which recapitulates clinically important physiological hallmarks of COVID-19-induced cardiac injury.

Data availability statement

The data cannot be made publicly available upon publication because they contain sensitive personal information. The data that support the findings of this study are available upon reasonable request from the authors.

Supplementary data available at https://doi.org/10.1088/1758-5090/ae38d7/data1.

Supplementary Video 1 available at https://doi.org/10.1088/1758-5090/ae38d7/data2.

Supplementary Video 2 available at https://doi.org/10.1088/1758-5090/ae38d7/data3.

Supplementary Video 3 available at https://doi.org/10.1088/1758-5090/ae38d7/data4.

Supplementary Video 4 available at https://doi.org/10.1088/1758-5090/ae38d7/data5.

Supplementary Video 5 available at https://doi.org/10.1088/1758-5090/ae38d7/data6.

Supplementary Video 6 available at https://doi.org/10.1088/1758-5090/ae38d7/data7.

Supplementary Video 7 available at https://doi.org/10.1088/1758-5090/ae38d7/data8.

Supplementary Video 8 available at https://doi.org/10.1088/1758-5090/ae38d7/data9.

Acknowledgments

CG was supported by a UTS Seed Funding and Catholic Archdiocese of Sydney Grant for Adult Stem Cell Research, a Heart Research Institute Fellowship, Heart Research Australia, a Perpetual IMPACT Grant, and the Ian Potter Foundation. CLCM was supported by a NSW Waratah Scholarship. MDJ is supported by a UTS Chancellor's Research Fellowship and the National Health and Medical Research Council (NHMRC) (2011467).

Author contributions

Matt D Johansen 0000-0001-5553-5270
Conceptualization (equal), Data curation (equal), Formal analysis (equal), Investigation (equal), Methodology (equal), Validation (equal), Writing – original draft (equal), Writing – review & editing (equal)

Clara Liu Chung Ming
Conceptualization (equal), Data curation (equal), Formal analysis (equal), Investigation (equal), Methodology (equal), Visualization (lead), Writing – original draft (lead), Writing – review & editing (equal)

Philip M Hansbro
Funding acquisition (equal), Resources (equal), Supervision (equal), Writing – review & editing (supporting)

Carmine Gentile 0000-0002-3689-4275
Conceptualization (equal), Data curation (equal), Funding acquisition (lead), Investigation (equal), Methodology (equal), Project administration (lead), Resources (equal), Software (equal), Supervision (lead), Validation (equal), Writing – review & editing (equal)

References

Cawood R, Harrison S M, Dove B K, Reed M L and Hiscox J A 2007 Cell cycle dependent nucleolar localization of the coronavirus nucleocapsid protein *Cell Cycle* **6** 863–7

Chen L, Li X, Chen M, Feng Y and Xiong C 2020 The ACE2 expression in human heart indicates new potential mechanism of heart injury among patients infected with SARS-CoV-2 *Cardiovasc. Res.* **116** 1097–100

Chung Ming C L *et al* 2024 3D *in vitro* modelling of post-partum cardiovascular health reveals unique characteristics and signatures following hypertensive disorders in pregnancy *Biol. Sex Differ.* **15** 94

Figtree G A, Bubb K J, Tang O, Kizana E and Gentile C 2017 Vascularized cardiac spheroids as novel 3D *in vitro* models to study cardiac fibrosis *Cells Tissues Organs* **204** 191–8

Gao T, Gao Y, Liu X, Nie Z, Sun H, Lin K, Peng H and Wang S 2021 Identification and functional analysis of the SARS-COV-2 nucleocapsid protein *BMC Microbiol.* **21** 58

Hanson P J *et al* 2022 Characterization of COVID-19-associated cardiac injury: evidence for a multifactorial disease in an autopsy cohort *Lab. Invest.* **102** 814–25

Hua X, Wang Y Y, Jia P, Xiong Q, Hu Y, Chang Y, Lai S, Xu Y, Zhao Z and Song J 2020 Multi-level transcriptome sequencing identifies COL1A1 as a candidate marker in human heart failure progression *BMC Med.* **18** 2

Jamoussi A, Messaoud L, Jarraya F, Rachdi E, Ben Mrad N, Yaalaoui S, Besbes M, Ayed S and Ben Khelil J 2023 Interleukin6 prediction of mortality in critically ill COVID19 patients: a prospective observational cohort study *PLoS One* **18** e0279935

Johansen M D *et al* 2020 Animal and translational models of SARS-CoV-2 infection and COVID-19 *Mucosal Immunol.* **13** 877–91

Johansen M D, Mahbub R M, Idrees S, Nguyen D H, Miemczyk S, Pathinayake P, Nichol K, Hansbro N G, Gearing L J and Hertzog P J 2022 Increased SARS-CoV-2 infection, protease, and inflammatory responses in chronic obstructive pulmonary disease primary bronchial epithelial cells defined with single-cell RNA sequencing *Am. J. Respir. Crit. Care Med.* **206** 712–29

Lam I C H *et al* 2024 Persistence in risk and effect of COVID-19 vaccination on long-term health consequences after SARS-CoV-2 infection *Nat. Commun.* **15** 1716

Li H, Liu S M, Yu X H, Tang S L and Tang C K 2020 Coronavirus disease 2019 (COVID-19): current status and future perspectives *Int. J. Antimicrob. Agents* **55** 105951

Li N, Zhu L, Sun L and Shao G 2021 The effects of novel coronavirus (SARS-CoV-2) infection on cardiovascular diseases and cardiopulmonary injuries *Stem Cell Res.* **51** 102168

Li X *et al* 2023 SARS-CoV-2-infected hiPSC-derived cardiomyocytes reveal dynamic changes in the COVID-19 hearts *Stem Cell Res. Ther.* **14** 361

Livak K J and Schmittgen T D 2001 Analysis of relative gene expression data using real-time quantitative PCR and the 2(-Delta delta C(T)) method *Methods* **25** 402–8

Lu R X Z *et al* 2022 Vasculature-on-a-chip platform with innate immunity enables identification of angiopoietin-1 derived peptide as a therapeutic for SARS-CoV-2 induced inflammation *Lab Chip* **22** 1171–86

Lu R X Z *et al* 2024a Cardiac tissue model of immune-induced dysfunction reveals the role of free mitochondrial DNA and the therapeutic effects of exosomes *Sci. Adv.* **10** eadk0164

Lu R X Z, Zhao Y and Radisic M 2024b The emerging role of heart-on-a-chip systems in delineating mechanisms of SARS-CoV-2-induced cardiac dysfunction *Bioeng. Transl. Med.* **9** e10581

Maccio U, Zinkernagel A S, Shambat S M, Zeng X, Cathomas G, Ruschitzka F, Schuepbach R A, Moch H and Varga Z 2021 SARS-CoV-2 leads to a small vessel endotheliitis in the heart *EBioMedicine* **63** 103182

Mills R J *et al* 2021 BET inhibition blocks inflammation-induced cardiac dysfunction and SARS-CoV-2 infection *Cell* **184** 2167–2182.e22

Ming L C, Patil R, Refaat A, Lal S, Wang X and Gentile C 2025 Acetylcholine-loaded nanoparticles protect against doxorubicin-induced toxicity in *in vitro* cardiac spheroids *Biofabrication* **17** 025023

Msemburi W, Karlinsky A, Knutson V, Aleshin-guendel S, Chatterji S and Wakefield J 2023 The WHO estimates of excess mortality associated with the COVID-19 pandemic *Nature* **613** 130–7

Mulay A *et al* 2021 SARS-CoV-2 infection of primary human lung epithelium for COVID-19 modeling and drug discovery *Cell Rep.* **35** 109055

Nguyen N, Nguyen H, Ukoha C, Hoang L, Patel C, Ikram F G, Acharya P, Dhillon A and Sidhu M 2022 Relation of interleukin-6 levels in COVID-19 patients with major adverse cardiac events *Bayl. Univ. Med. Cent. Proc.* **35** 6–9

Nikkhoo B *et al* 2023 Elevated interleukin (IL)-6 as a predictor of disease severity among Covid-19 patients: a prospective cohort study *BMC Infect. Dis.* **23** 311

Polonchuk L, Chabria M, Badi L, Hoflack J C, Figtree G, Davies M J and Gentile C 2017 Cardiac spheroids as promising *in vitro* models to study the human heart microenvironment *Sci. Rep.* **7** 7005

Qiu H, Li J, Li J, Li H and Y X 2023 COVID-19 and acute cardiac injury: clinical manifestations, biomarkers, mechanisms, diagnosis, and treatment *Curr. Cardiol. Rep.* **25** 817–29

Roche C D, Lin H, Huang Y, DE Bock C E, Beck D, Xue M and Gentile C 2023 3D bioprinted alginate-gelatin hydrogel patches containing cardiac spheroids recover heart function in a mouse model of myocardial infarction *Bioprinting* **30** e00263

Sato K, Sinclair J E, Sadeghirad H, Fraser J F, Short K R and Kulasinghe A 2021 Cardiovascular disease in SARS-CoV-2 infection *Clin. Transl. Immunol.* **10** e1343

Scherer K M *et al* 2022 SARS-CoV-2 nucleocapsid protein adheres to replication organelles before viral assembly at the Golgi/ERGIC and lysosome-mediated egress *Sci. Adv.* **8** eabl4895

Shao X, Zhang X, Zhang R, Zhu R, Hou X, Yi W, Wu F, Hao L and Feng R 2022 The atlas of ACE2 expression in fetal and adult human hearts reveals the potential mechanism of heart-injured patients infected with SARS-CoV-2 *Am. J. Physiol. Cell Physiol.* **322** C723–C38

Sharma P, Ming C L C and Gentile C 2022a In vitro modeling of myocardial ischemia/reperfusion injury with murine or human 3D cardiac spheroids *STAR Protocols.* **3** 101751

Sharma P, Ming C L C, Wang X, Bienvenu L A, Beck D, Figtree G, Boyle A and Gentile C 2022b Biofabrication of advanced in vitro 3D models to study ischaemic and doxorubicin-induced myocardial damage *Biofabrication* **14** 025003

Shen Y, Chen M, Gu W, Wan J, Cheng Z, Shen K, Zhang W, HE J, WanG Y and Deng X 2023 The molecular mechanism of cardiac injury in SARS-CoV-2 infection: focus on mitochondrial dysfunction *J. Infect. Public Health* **16** 746–53

Verdecchia P, Cavallini C, Spanevello A and Angeli F 2020 The pivotal link between ACE2 deficiency and SARS-CoV-2 infection *Eur. J. Intern. Med.* **76** 14–20

Wang D *et al* 2020 Clinical characteristics of 138 hospitalized patients with 2019 novel coronavirus-infected pneumonia in wuhan, China *JAMA* **323** 1061–9

Worldometer 2024 *COVID-19 CORONAVIRUS PANDEMIC* (available at: www.worldometers.info/coronavirus/)

Yang L *et al* 2021a An immuno-cardiac model for macrophage-mediated inflammation in COVID-19 Hearts *Circ. Res.* **129** 33–46

Yang L, Nilsson-payant B E, Han Y, Jaffré F, Zhu J, Wang P, Zhang T, Redmond D, Houghton S and Møller R 2021b Cardiomyocytes recruit monocytes upon SARS-CoV-2 infection by secreting CCL_2 *Stem Cell Rep.* **16** 2274–88